Chemical Engineering Journal 165 (2010) 10–16

Contents lists available at ScienceDirect

Chemical Engineering Journal

journal homepage: www.elsevier.com/locate/cej

Review

Tannic acid adsorption on amino-functionalized magnetic mesoporous silica

Jiahong Wang[a,b], Shourong Zheng[a], Jingliang Liu[a], Zhaoyi Xu[a,*]

[a] State Key Laboratory of Pollution Control and Resource Reuse, and School of the Environment, Nanjing University, 22 Hankou Road, Nanjing, Jiangsu 210093, PR China
[b] College of Resource and Environment, Shaanxi University of Science & Technology, Xi'an 710021, PR China

ARTICLE INFO

Article history:
Received 13 May 2010
Received in revised form 26 August 2010
Accepted 26 August 2010

Keywords:
Tannic acid
Adsorption
Magnetic mesoporous silica
Amino-functionalization

ABSTRACT

Amino-functionalized magnetic mesoporous silica (magMCM-41-NH_2) was prepared and adsorption of organic pollutant tannic acid (TA) from aqueous solution on the resulting material was investigated. The adsorbent was characterized by elemental analysis, X-ray diffraction (XRD), transmission electron microscopy (TEM), N_2 adsorption-desorption, IR spectroscopy, Zeta potential measurements and vibration sample magnetometer (VSM). Characterization results showed that magMCM-41-NH_2 had ordered mesoporous structure with amino group content of 4.57 wt%, BET surface area of 668 m^2/g and the pore volume of 0.525 cm^3/g. Batch adsorption tests indicated that magMCM-41-NH_2 adsorbent exhibited high adsorption affinity towards aqueous TA with a maximum adsorption capacity of 510.2 mg/g. The Freundlich model could fit the adsorption isotherm of TA over magMCM-41-NH_2 very well, implying that adsorption process is heterogeneous. TA adsorption on magMCM-41-NH_2 could be well described by the pseudo-second-order kinetics. Adsorption of TA on the adsorbent was found to be strongly dependent on pH and ionic strength, suggesting that electrostatic interaction played a crucial role in TA adsorption. X-ray photoelectron spectroscopy (XPS) analysis confirmed the formation of complex compound between TA and surface amino groups of magMCM-41-NH_2 upon adsorption.

© 2010 Elsevier B.V. All rights reserved.

1. Introduction

Phytic substances, such as tannic acid (TA) and gallic acid, are naturally occurring organic matters in surface and ground water, resulting from the decomposition of natural organic matter [1]. As a water soluble polyphenolic compounds, TA is considered to be toxic to aquatic organism, such as algae, fish and invertebrates. In particular, the presence of TA in drinking water may act as the precursor of carcinogenic disinfection byproducts (DBPs) [1–4]. Hence, minimization and removal of TA in water is of practical importance and interest.

A variety of treatment techniques have been developed to remove TA in water, including chemical oxidation, electrochemical method, coagulation, ultrafiltration, adsorption, and biological method [5–9]. Among them, the adsorption method has been intensively investigated. For example, zirconium pillared clay, chitosan, cationic surfactant-modified bentonite clay, resin, and activated carbon have been found to be effective for the adsorptive removal of aqueous TA [3,4,10,11]. However, the separation process of adsorbents from aqueous solution after saturated adsorption is usually complex and time-consuming.

Recently, magnetic mesoporous silica combining the advantage of mesoporous structure and sufficient magnetization has received great attention in environmental remediation. The magnetic mesoporous silica adsorbent has the unique large surface area, ordered mesoporous structure and narrow pore size distribution, which make it suitable candidate for pollutant adsorption in aqueous solution. Additionally, the magnetic mesoporous silica is susceptible to surface functionalization due to its abundant surface silanol groups. After saturated adsorption, moreover, magnetic mesoporous silica can be easily separated from mixture solution by external magnetic field. It should be emphasized that as an inert matrix mesoporous silica usually displays low adsorption capacity towards pollutants. Alternatively, surface functionalization of mesoporous silica by active amino group [12,13] or thio-group [14] may lead to markedly enhanced adsorption. Previous researches on magnetic mesoporous silica adsorbents mainly focused on the removal of aqueous heavy metal [15,16], and only a few studies have been conducted on adsorption of organic pollutants in water. For example, Tian et al. synthesized the magnetic hexagonal mesoporous which can remove DDT from aqueous solution [17]. Deng et al. prepared a superparamagnetic microsphere with an Fe_3O_4@SiO_2 core and mesoporous SiO_2 shell and observed fast removal of microcystins in water [18]. To our best knowledge, however, no study has been conducted on TA adsorption to surface functionalized magnetic mesoporous silica adsorbents thus far.

* Corresponding author. Tel.: +86 025 8359 5831.
E-mail address: zhaoyixu@nju.edu.cn (Z. Xu).

1385-8947/$ – see front matter © 2010 Elsevier B.V. All rights reserved.
doi:10.1016/j.cej.2010.08.066

In this study, magnetic mesoporous silica were prepared and further functionalized by aminopropyl group. The physical, chemical, and structural properties of the magnetic mesoporous silica were characterized by XRD, IR spectroscopy, elemental analysis, N_2 adsorption-desorption and Zeta potential measurement. The adsorption of aqueous TA on the synthesized adsorbent was evaluated by batch experiments and adsorption kinetic tests. The impacts of pH and ionic strength on TA adsorption were investigated. The mechanism of TA adsorption to the adsorbent was also proposed based on batch adsorption and XPS analysis results.

2. Materials and methods

2.1. Materials

TA and 3-aminopropyltrimethoxysilane supplied by Aldrich Chemical Co. were used as received without further purification.

2.2. Preparation of magnetic mesoporous silica

Magnetic MCM-41 was prepared by a two-step synthesis procedure as described by Chen et al. [19]. To prepare the magnetic Fe_3O_4 nanoparticles, 1.5 g of iron(III) chloride and 0.6 g iron(II) chloride were dissolved in 10 mL of deionized water purged by a N_2 flow (60 mL/min) for 0.5 h. The resulting mixture was then added under nitrogen to 50 mL solution of 1.0 mol L^{-1} $NH_3{\cdot}H_2O$ solution containing 0.2 g of cetyltrimethylammonium bromide (CTABr) under sonication. After reaction for 30 min, the colloidal iron oxide nanoparticles were recovered magnetically. The magnetic MCM-41 sample was prepared by adding the as-synthesized Fe_3O_4 nanoparticles to 1.0 L solution containing 640 mL deionized water (degassed with nitrogen), 360 mL of 15 mol L^{-1} $NH_3{\cdot}H_2O$ ammonia solution and 5.8 g CTABr under vigorous mechanical stirring and N_2 protection. After reaction for 30 min, 23.2 mL tetraethyl orthosilicate was added dropwise and the mixture further reacted at 30 °C for 24 h. The magnetic MCM-41 was magnetically collected. The organic template CTABr was removed by Soxhlet extraction with ethanol for 36 h followed by drying at 70 °C under vacuum for 12 h. The resulting material is referred to as magMCM-41.

The surface functionalized magMCM-41 was prepared by the post-grafting method. Briefly, 2.0 g of magMCM-41 particles was suspended in 100 mL of dry toluene containing 3.0 mL of 3-aminopropyltrimethoxysilane with mechanical stirring under N_2 protection. The mixture was refluxed at 110 °C for 12 h, then magnetically separated, followed by repeated washing by ethanol and drying at 70 °C under vacuum for 12 h. The amino-functionalized magMCM-41 is denoted as magMCM-41-NH_2. The Fe_3O_4 content in the composite material determined using the method described by Liu et al. [20] was 10.5 wt%.

2.3. Material characterization

Small angle X-ray diffraction (XRD) patterns of the samples were recorded on a powder diffraction-meter (D/max-RA, Rigaku), operating with a Cu anode at 40 kV and 40 mA in the range of 0.5–5° with a speed of 2 min^{-1}. Wide angle XRD patterns of the samples were measured in the range of 15–70°. Fourier transform-infrared (FT-IR) spectra were recorded in a FT-IR spectrometer (Nicolet 5700, Thermo Nicolet) at 2 cm^{-1} resolution. N_2 adsorption-desorption isotherms were collected on a Micromeritics ASAP 2200 instrument. TEM observation was performed on a transmission electron microscope (H-800, Hitachi). Magnetic properties of the samples were measured by a vibration sample magnetometer (Lake Shore 7410, Lake Shore) under magnetic fields up to 10 kOe. The TGA curves were taken by using a thermo gravimetric analyzer (Pyris 1 TGA, PerkinElmer) under a stable N_2 flow. The temperature studied ranged from 25 to 750 °C at a ramping rate of 20 °C/min^{-1}. Carbon, hydrogen and nitrogen contents of the samples were determined with elemental analyzer (CHN-O-Rapid, Heracus). X-ray photoelectron spectroscopy (XPS) measurement was conducted with a spectrometer (Escalab 250, Thermo-VG Scientific) with a Al KR X-ray source to determine the C, N, and O atoms present on the surface. All binding energies were referenced to the neutral C_{1s} peak at 284.6 eV to compensate for the surface charging effects. The Zeta potentials of the materials were determined according to reference [21].

2.4. Adsorption of TA

The batch experiments were carried out to evaluate TA adsorption isotherms over magMCM-41-NH_2. Typically, 10 mg of magMCM-41-NH_2 was added to 60 mL flask receiving 50 mL of TA solution with initial concentrations varying from 20 to 200 mg/L with pH 6.98–7.36. The flasks were transferred into an incubator, in which the tubes were shaken at 25 °C for 24 h. After reaching adsorption equilibrium, the adsorbent particles were magnetically separated from the aqueous solution and the residual concentrations of TA in the aliquot were determined using a UV–vis spectrometer with detecting wavelength at 278 nm [1]. The equilibrium adsorption amounts of TA were calculated according to Eq. (1):

$$q_e = \frac{(C_0 - C_e)V}{M} \quad (1)$$

where q_e is the amount of TA adsorbed at equilibrium, C_0 is the initial TA concentration, C_e is the equilibrium TA concentration, V is the volume of TA solution, and M is the adsorbent mass.

For adsorption kinetics at 25 °C, 100 mg of magMCM-41-NH_2 was fast introduced into a 500 mL three neck flask containing 500 mL of TA solution with an initial TA concentration of 50, 100, or 200 mg/L, respectively under strong mechanic stirring. 4 mL of solution was withdrawn at different time intervals. After magnetic separation of the adsorbent particles, the residual TA concentration was spectrophotometrically determined.

The pH effect on TA adsorption was investigated in a pH range from 3 to 10. A series of flasks containing 10 mg of magMCM-41-NH_2 and 50 mL of 100 mg/L TA solution with different pH pre-adjusted with 0.1 mol/L HCl or NaOH solution were shaken at 25 °C for 24 h. The residual TA concentrations were determined spectrophotometrically and adsorption amounts of TA were calculated according to Eq. (1).

Effect of background electrolyte on TA adsorption was studied by dispersing 10 mg of adsorbents in 50 mL NaCl, KCl or $CaCl_2$ solution (40–240 mg/L) containing 100 mg/L TA at pH 7.2.

3. Results and discussion

3.1. Material characterization

The crystalline structure of the magnetic nanoparticle was characterized using wide angle XRD and the result is shown in Fig. S1. The diffraction peaks with 2θ at 30.4°, 35.6°, 43.3°, 57.3°, and 62.8° were observed, indicative of a cubic spinel structure of the magnetite. The small angle XRD patterns of magMCM-41 and magMCM-41-NH_2 were compared in Fig. 1. For magMCM-41, three well-resolved diffraction peaks with 2θ at 2.22°, 3.88° and 4.42°, indexed to (1 0 0), (1 1 0) and (1 2 0) diffraction, were clearly observed, indicative of the presence of hexagonal mesoporous structure. The diffraction peaks are also visible in the XRD pattern of magMCM-41-NH_2, reflecting that the ordered hexagonal structure retained unchanged after aminopropyl group functionalization. Notably, the peak intensity of magMCM-41-NH_2 decreased

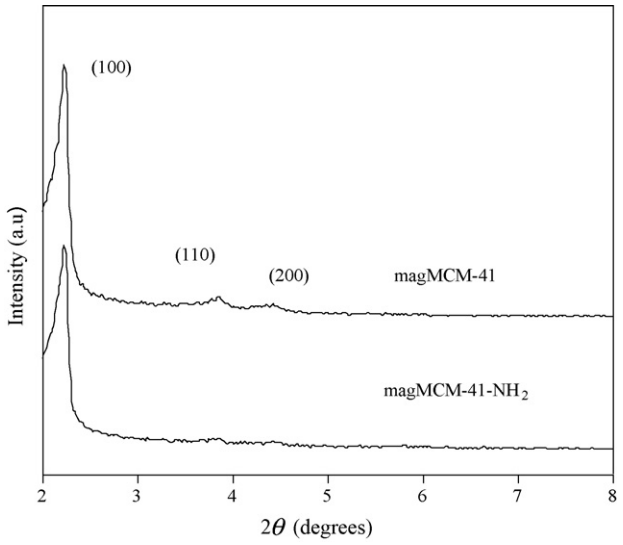

Fig. 1. Powder X-ray diffraction (XRD) patterns of magMCM-41 and magMCM-41-NH_2.

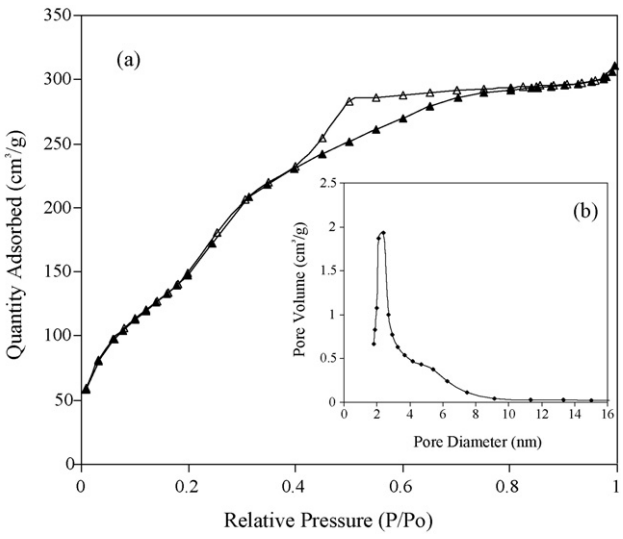

Fig. 3. (a) N_2 adsorption-desorption isotherm and (b) Pore size distribution of magMCM-41-NH_2.

in comparison with magMCM-41, likely resulting from the contrast matching between the SiO_2 framework and aminopropyl groups on mesoporous SiO_2 surface upon surface functionalization [22]. The ordered mesoporous structure of magMCM-41-NH_2 was further confirmed by TEM observation, as shown in Fig. 2. Iron oxide nanoparticles with diameter of about 10 nm were incorporated into mesoporous silica.

N_2 adsorption-desorption isotherm and pore size distribution of magMCM-41-NH_2 are presented in Fig. 3. At relative pressure range of 0.5–0.8, typical capillary condensation was observed, suggesting the presence of mesopores in magMCM-41-NH_2. The BET surface area was calculated to be 668 m^2/g and the pore volume was 0.525 cm^3/g. From N_2 adsorption, the presence of micropore was observed and the ration of micropore to mesopore was 0.32, probably due to the aminopropyl functionalization in mesopores, giving rise to the narrowed pore diameter. The pore size distribution showed that magMCM-41-NH_2 consisted of mesopores with the most probable pore diameter centered at 2.4 nm.

The IR spectrum of magMCM-41-NH_2 is illustrated in Fig. S2. The IR band at 590 cm^{-1} is assigned to the Fe–O vibration associated with iron oxide. The IR bands centered at 463, 804, 1074 cm^{-1} are characteristic of the stretching and deformation vibrations of SiO_2. The bands around 2800–3025 cm^{-1} resulted from the stretching vibration of methylene groups and the bands in the region of 1460–1600 cm^{-1} were attributed to the bending vibration of amino groups, reflecting that aminopropyl groups were incorporated to the magMCM-41. The finding was further confirmed by the thermal analysis results shown in Fig. S3. The weight loss (3.4 wt%) below 200 °C was attributed to the water loss and the weight loss (1.34 wt%) above 600 °C was assigned to the loss of structural water of the adsorbent. A weight loss of 17.6 wt% at the temperature range of 200–600 °C resulted from the decomposition of aminopropyl groups bound to the adsorbents. Chemical analysis indicated that the content of C, H, N in magMCM-41-NH_2 were 11.7 wt%, 4.6 wt% and 2.1 wt% respectively, which was in good agreement with the result of thermal analysis.

Zeta potentials of magMCM-41 and magMCM-41-NH_2 are shown in Fig. 4. Zeta potentials of magMCM-41decrease with solution pH and the isoelectric point (IEP) is about 2.0, which is nearly identical to that of amorphous silica [23]. In contrast, the IEP of the material was found to be 5.8, reflecting that aminopropyl functionlization led to increased IEP [24].

The magnetization curve of magMCM-41-NH_2 is plotted in Fig. S4. The saturation magnetization of magMCM-41-NH_2 is

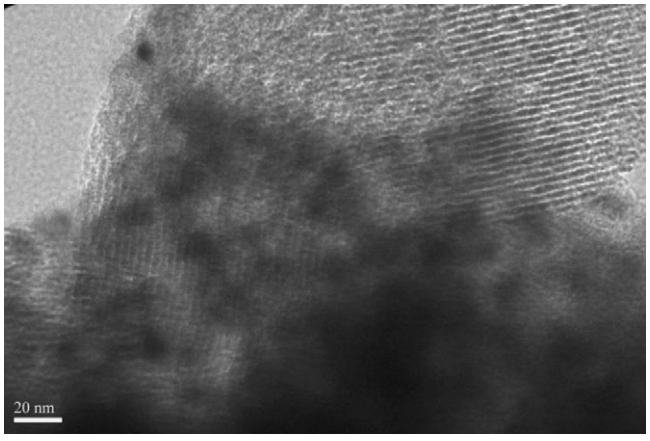

Fig. 2. TEM images of magMCM-41-NH_2.

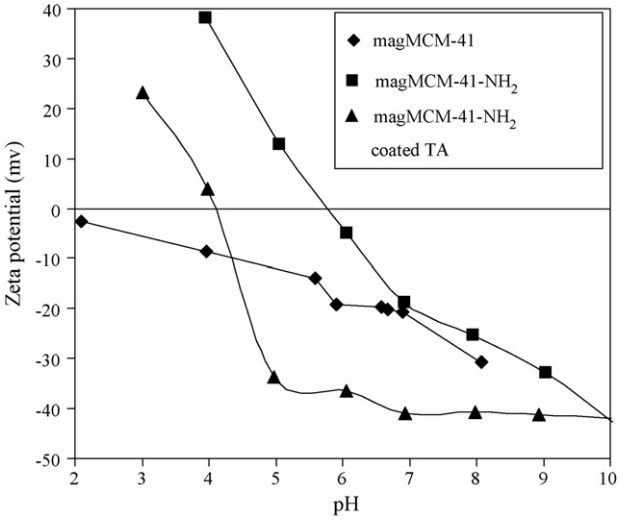

Fig. 4. Zeta potentials of magMCM-41, magMCM-41-NH_2 and magMCM-41-NH_2 coated with TA as a function of pH.

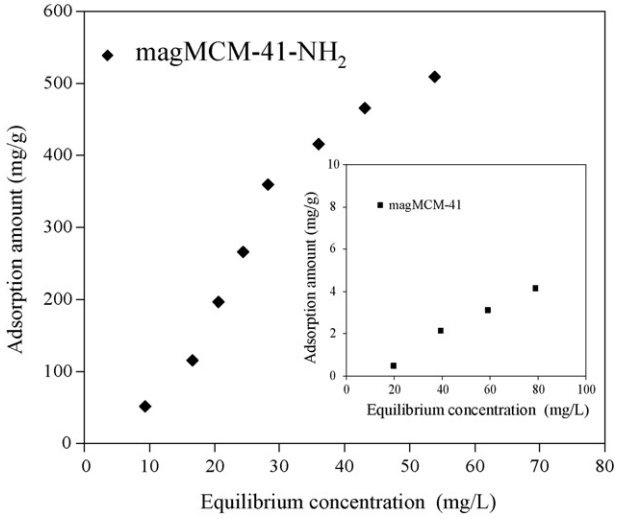

Fig. 5. Adsorption isotherms of TA over magMCM-41-NH_2 plotted as equilibrium adsorption amount vs equilibrium concentration at pH 6.98–7.36.

8.96 emu/g, and a low coercivity of 5.12 Oe and remanence of 0.095 emu/g were recorded, suggesting that the magMCM-41-NH_2 is superparamagnetic and easily separated under external magnetic fields. In a typical adsorption run, recovery of loaded adsorbent via magnetic separation was achieved within 5 min.

3.2. Adsorption isotherms

Adsorption isotherms of TA on the magMCM-41-NH_2 and magMCM-41 are compared in Fig. 5. magMCM-41 showed negligible adsorption for TA, whereas the maximum adsorption amount over magMCM-41-NH_2 within the tested concentration range was 510.2 mg/g, indicative of a substantially enhanced TA adsorption upon surface functionalization by aminopropyl groups.

In principle, the Freundlich adsorption model is generally used to describe the heterogeneous adsorption behavior:

$$\log q_e = \frac{1}{n}\log C_e + \log K_f \quad (2)$$

where q_e is the equilibrium adsorption amount at TA equilibrium concentration C_e, K_f is Freundlich coefficient characteristic of the adsorption affinity of the adsorbent, and n is the linearity index [25].

The fitting parameters for TA adsorption isotherms using Freundlich equation are listed in Table 1. TA adsorption on magMCM-41-NH_2 and magMCM-41 could be well described by the Freundlich adsorption model with R^2 higher than 0.96. The results also suggest the heterogeneous adsorption sites in the adsorbent for TA adsorption [26], likely attributed to the heterogeneous distribution of amino groups anchored on the adsorbent [27,28]. Freundlich coefficients of TA adsorption on magMCM-41 and magMCM-41-NH_2 were calculated to be 0.0044 and 2.8, respectively, indicating that surface functionalization markedly enhanced TA adsorption.

Table 1
Adsorption parameters of TA adsorption to the adsorbents.

Adsorbents	K	n	R^2
magMCM-41-NH_2	2.80	0.73	0.96
magMCM-41	0.0044	0.62	0.95

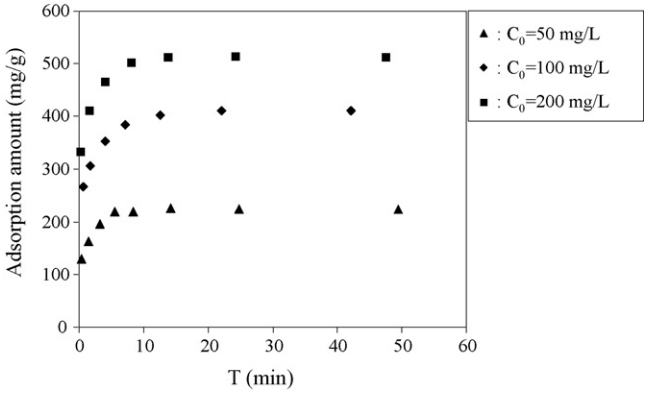

Fig. 6. Time resolved HA adsorption to magMCM-41-NH_2 at different initial TA concentrations at pH 6.71–6.86.

3.3. Adsorption kinetics

The dependence of TA adsorption on adsorption time is shown in Fig. 6. The adsorption of TA with initial concentrations of 50, 100 and 200 mg/L reached adsorption equilibrium within 5.5, 12.6 and 13.9 min respectively, suggesting a fast adsorption process at low initial TA concentration.

Given a heterogeneous adsorption process, the pseudo-first-order or pseudo-second-order model is usually adopted to follow the mass transfer process. For pseudo-first-order kinetics, the adsorption process can be described by Lagergren's rate equation [3]:

$$\log(q_e - q_t) = \log q_e - \frac{k_1}{2.303}t \quad (3)$$

where q_e is the adsorption amount, q_t is the adsorption amount at time t and k_1 is the pseudo-first-order rate constant.

The pseudo-second-order kinetics based on adsorption capacity can be expressed as follows (4):

$$\frac{t}{q_t} = \frac{1}{k_2 q_e^2} + \frac{1}{q_e}t \quad (4)$$

where q_e is the adsorption amount, q_t is the adsorption amount at time t and k_2 is the pseudo-second-order rate constant.

Simulation results of TA adsorption to magMCM-41-NH_2 based on the pseudo-first-order kinetics and pseudo-second-order kinetics are shown in Fig. S5a and Fig. S5b, and the fitting parameters are listed in Table 2. As shown in Fig. S5a, the plot of $\log(q_e - q_t)$ versus t did not give a linear relation, suggesting that pseudo-first-order kinetic model cannot well describe TA adsorption process over magMCM-41-NH_2. On the contrast, the plot in Fig. S5b presents linear relation with R^2 higher than 0.99. In addition, TA adsorption amounts obtained from experimental data are approximately identical to those calculated from fitting results, further indicating that TA adsorption process on magMCM-41-NH_2 obeys pseudo-second-order kinetics. The adsorption rate constants calculated based on the pseudo-second-order kinetics are 1.38×10^{-2}, 1.25×10^{-2} and 7.22×10^{-3} g/(mg min) at initial concentrations of 50, 100 and 200 mg/L respectively, reflecting a relatively slow adsorption process at a high initial TA concentration. At low initial concentration, TA adsorption amount over the adsorbent is expected to be low, which can be facially achieved by adsorption on the pore mouth region. At high initial concentration, however, TA molecule penetrates deeply into the mesopore to approach amino groups due to complete occupation of amino groups in the pore mouth region, leading to a long diffusion path and consequently low adsorption rate [29].

Table 2
Fitting parameters of TA adsorption to magMCM-41-NH_2 using pseudo-second order kinetic models.

C_0 (mg/L)	q_{exp} (mg/g)	First order kinetics			Second order kinetics		
		K_1 (1/min)	q_{cal} (mg/g)	R^2	K_2 (g/(mg min))	q_{cal} (mg/g)	R^2
50	226.13	0.2665	71.04	0.99	1.38×10^{-2}	227.27	0.99
100	410.76	0.2591	149.11	0.97	1.25×10^{-2}	416.67	0.99
200	512.57	0.2691	172.38	0.99	7.22×10^{-3}	526.32	0.99

3.4. Effect of ionic strength and solution pH

The cations Na^+, K^+, Ca^{2+} present in natural water may interact with TA, which affects TA adsorption on the adsorbent. Fig. 7 displays the effect of ionic strength (Na^+, K^+ and Ca^{2+}) on TA adsorption to magMCM-41-NH_2 adsorbent. Results show that the presence of the tested cations led to enhanced TA adsorption on magMCM-41-NH_2. In addition, TA adsorption amount gradually increased with increasing concentration of Na^+, K^+ and Ca^{2+}, and the enhanced TA adsorption was order as $Ca^{2+} > K^+ > Na^+$. The enhancement of TA adsorption by coexisting cations is likely attributed to the weakening of the repulsive interaction between adsorbed TA molecules on the surface of the adsorbent and TA molecules in solution. Moreover, Na^+, K^+ and Ca^{2+} ions may directly interact with TA to form complex compounds, hence the cations bounded to the adsorbent may adsorb aqueous TA, leading to enhanced TA adsorption. The strong dependence of TA adsorption on ionic strength further implies that the electrostatic interaction plays a crucial role in TA adsorption on magMCM-41-NH_2.

The effect of pH on TA adsorption over magMCM-41-NH_2 is descried in Fig. 8. In the tested pH range, TA adsorption amount was relatively high at pH 4.53–6.95 with the maximum adsorption amount at pH 5.64. At pH below 4.53, TA adsorption sharply decreased with the decrease of pH, whereas at pH higher than 5.64 TA adsorption decreased with the increasing of pH. As demonstrated by TA adsorption over magMCM-41, negligible TA adsorption over SiO_2 surface is rationally expected and TA adsorption over magMCM-41-NH_2 is primarily driven by surface complexation with amino groups. The pK_a value of aminopropyl group is 9.8 and the aminopropyl groups are thus supposed to be positively charged by protonation at pH lower than 9.8. It is noteworthy that the IEP of TA is around 4.5. At pH above 4.5, therefore, dissociated TA molecules exist as anions, leading to a strong electrostatic interaction with positively charged amino groups in magMCM-41-NH_2 and thus to high TA adsorption capacity. However, at pH above 5.8, increasing solution pH leads to decreased protonation of aminopropyl group, which may decrease the electrostatic force between the TA molecules and adsorbents and cause the suppressed TA adsorption. The high TA adsorption amount at pH above 5.8 further suggests that in addition to the electrostatic interaction, other driving force such as the hydrogen bonding between aminopropyl and disassociated phenolic group may gradually play a dominant role in TA adsorption. At pH below 4.5, in contrast, TA molecules are present in a neutral form. In this case a weak hydrogen bonding interaction might be responsible for TA adsorption, which results in markedly decreased adsorption amount.

3.5. Adsorption mechanism

Zeta potentials of magMCM-41-NH_2 before and after adsorption of TA are shown in Fig. 4. TA adsorption led to decreased Zeta potentials in the tested pH range. Additionally, the IEP of the TA loaded magMCM-41-NH_2 was 4.10, which suggests that TA molecules have been conjugated on the adsorbent. The significant difference of Zeta potentials of the adsorbent before and after adsorption was found to be at pH 4–7, which may account for the enhanced TA adsorption.

The interaction between TA molecule and the surface amino groups of magMCM-41-NH_2 was further verified by XPS results. The C_{1s} spectra and N_{1s} spectra of magMCM-41-NH_2 before and after adsorption are compared in Fig. 9. For magMCM-41-NH_2 (see Fig. 9a and b), only one peak with binding energy of 284.8 eV was observed in C_{1s} spectra of magMCM-41-NH_2, assignable to C–C carbon from the aminoproyl group grafted on the adsorbent surface. After TA adsorption, two new peaks were found at the binding energy of 286.5 and 288.8 eV attributed to C–O and $-C_6H_4-CO-O$ carbon respectively, indicating that TA is adsorbed on the adsorbents. The interaction between TA and aminopropyl group was further confirmed by the N_{1s} spectra of magMCM-41-NH_2 before and after TA adsorption. As shown in Fig. 9c and d, the binding energies of the N_{1s} core-level spectra were centered at 399.6 and

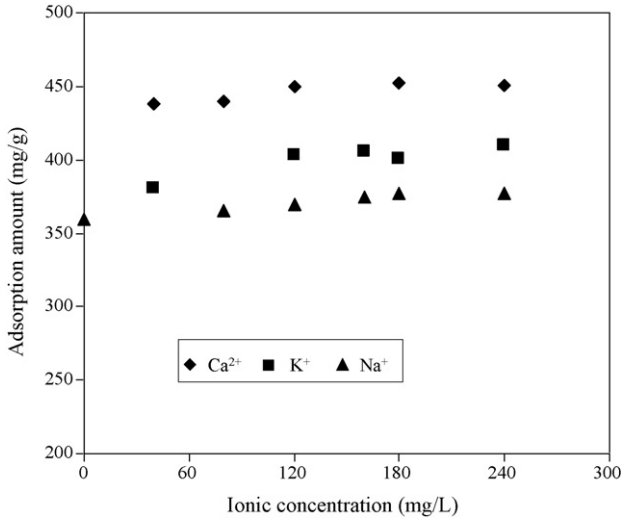

Fig. 7. Effect of ionic strength on TA adsorption to magMCM-41-NH_2 at 25 °C.

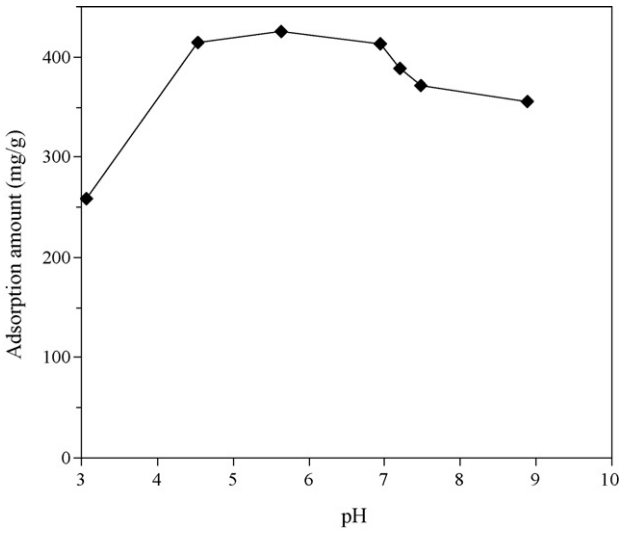

Fig. 8. Effect of pH on TA adsorption to magMCM-41-NH_2 at 25 °C.

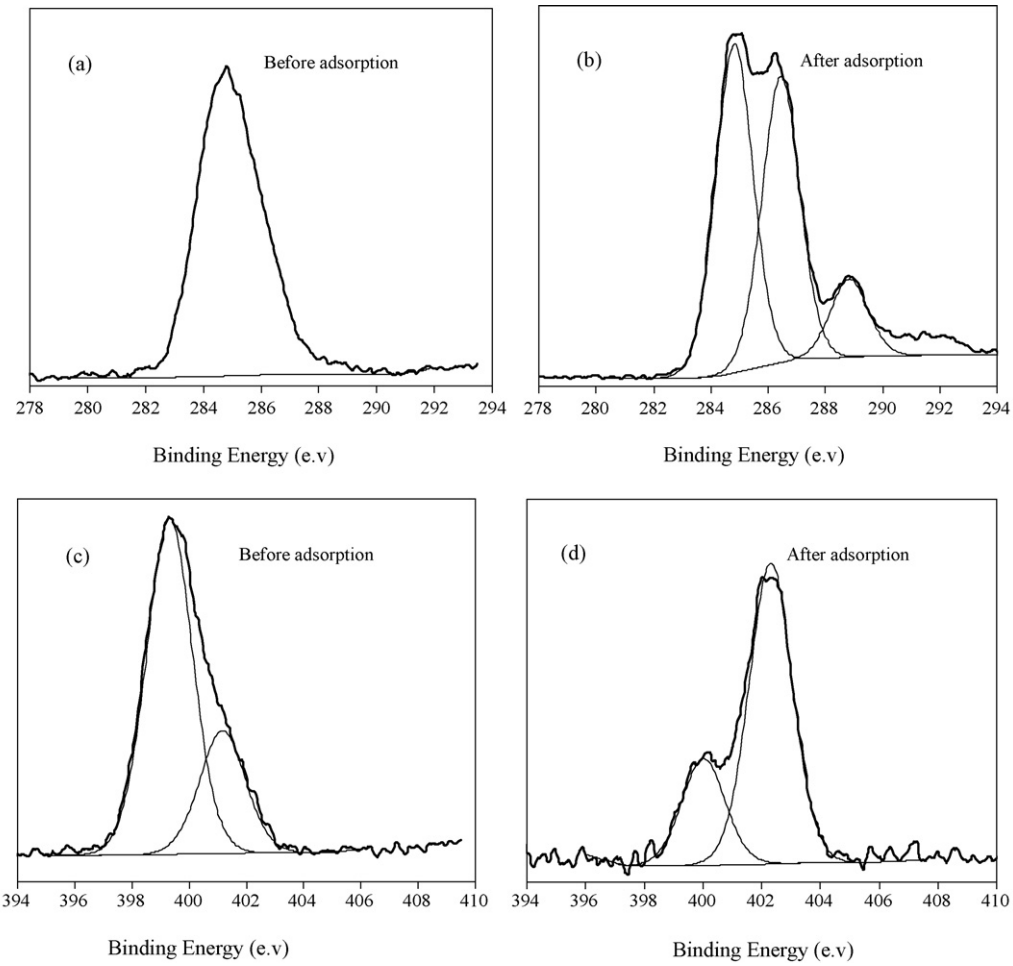

Fig. 9. XPS C1s spectra of magMCM-41-NH_2 (a) before and (b) after TA adsorption, and N1s spectra of magMCM-41-NH_2 (c) before and (d) after TA adsorption.

401.6 eV respectively, characteristic of the coexistence of neutral amino (-NH_2) and protonated amino groups (NH_3^+). The presence of protonated amino groups likely results from the hydrogen bonding interaction between surface amino groups (–NH_2) and surface silanol groups [30]. Upon TA adsorption, two peaks characteristic of neutral amino and protonated amino group were also visible on the N_{1s} spectra. However, TA adsorption led to the decrease in the ratio of neutral amino group content to protonated amino group content from 2.75 to 0.35, indicating that TA molecule is conjugated with the amino group of magMCM-41-NH_2 to form a new complex via a acid-base interaction. The result clearly indicates that TA is adsorbed on the magMCM-41-NH_2 adsorbent by complexing with aminopropyl groups.

4. Conclusions

In this study, amino-functionalized magnetic mesoporous silica magMCM-41-NH_2 was synthesized and adsorption of aqueous TA to the adsorbent was investigated. Characterization results showed that aminopropyl group was successfully grafted on magMCM-41, and the amino-functionalized adsorbent possessed ordered mesoporous structure and sufficient magnetization for magnetic separation purpose. The presence of the amino group in the adsorbent accounts for the highly effective adsorption of TA in aqueous solution. Fast adsorption of TA to magMCM-41-NH_2 can be achieved due to the mesoporous nature of the adsorbent. TA adsorption is dependent on solution pH and is observed to be favored in the pH range of 4.53–6.95. Coexisting cations (Na^+, K^+, and Ca^{2+}) in aqueous solution result in enhanced TA adsorption. XPS analysis indicates that the formation of complex compound between amino groups of the adsorbent and TA may play an important role in TA adsorption. The present results imply that magMCM-41-NH_2 adsorbent is a promising adsorbent for adsorptive removal of aqueous TA in water and wastewater treatment.

Acknowledgements

This work was supported by the National Basic Research Program of China (973 program, Grant 2008CB418102), the National Natural Science Foundation of China (Grants 40402022 and 20877039) and Natural Science Foundation of Jiangsu Province, China (Grant SBK201040050).

Appendix A. Supplementary data

Supplementary data associated with this article can be found, in the online version, at doi:10.1016/j.cej.2010.08.066.

References

[1] J.H. An, S. Dultz, Adsorption of tannic acid on chitosan-montmorillonite as a function of pH and surface charge properties, Appl. Clay Sci. 36 (2007) 256–264.
[2] J.N. Wang, A.M. Li, L. Xu, Y. Zhou, Adsorption of tannic and gallic acids on a new polymeric adsorbent and the effect of Cu(II) on their removal, J. Hazard. Mater. 169 (2009) 794–800.
[3] M.Y. Chang, R.S. Juang, Adsorption of tannic acid, humic acid, and dyes from water using the composite of chitosan and activated clay, J. Colloid Interface Sci. 278 (2004) 18–25.

[4] T.S. Anirudhan, M. Ramachandran, Adsorptive removal of tannin from aqueous solutions by cationic surfactant-modified bentonite clay, J. Colloid Interface Sci. 299 (2006) 116–124.
[5] W.W. Li, X.D. Li, K.M. Zeng, Aerobic biodegradation kinetics of tannic acid in activated sludge system, Biochem. Eng. J. 43 (2009) 142–148.
[6] Y. Zhou, X.H. Xing, Z. Liu, L. Cui, A. Yu, Q. Feng, H. Yang, Enhanced coagulation of ferric chloride aided by tannic acid for phosphorus removal from wastewater, Chemosphere 72 (2008) 290–298.
[7] A. Buso, L. Balbo, M. Giomo, G. Farnia, G. Sandona, Electrochemical removal of tannins from aqueous solutions, Ind. Eng. Chem. Res. 39 (2000) 494–499.
[8] M. Pepi, L.R. Lampariello, R. Altieri, A. Esposito, G. Perra, M. Renzi, A. Lobianco, A. Feola, S. Gasperini, S.E. Focardi, Tannic acid degradation by bacterial strains *Serratia* spp. and *Pantoea* sp. isolated from olive mill waste mixtures, Int. Biodeter. Biodegr. 64 (2010) 73–80.
[9] P. Cañizares, Á. Pérez, R. Camarillo, J. Llanos, Tannic acid removal from aqueous effluents using micellar enhanced ultrafiltration at pilot scale, Desalination 200 (2006) 310–312.
[10] J. Rivera-Utrilla, C. Moreno-Castilla, E. Utrera-Hidalgo, F. Carrasco-Marin, Removal of tannic acid from aqueous solutions by activated carbons, Chem. Eng. J. 52 (1993) 37–39.
[11] V.P. Vinod, T.S. Anirudhan, Sorption of tannic acid on zirconium pillared clay, J. Chem. Tech. Biotech. 77 (2002) 92–101.
[12] J. Li, X. Miao, Y. Hao, J. Zhao, X. Sun, L. Wang, Synthesis, amino-functionalization of mesoporous silica and its adsorption of Cr(VI), J. Colloid Interface Sci. 318 (2008) 309–314.
[13] H. Yoshitake, T. Yokoi, T. Tatsumi, Adsorption of chromate and arsenate by amino-functionalized MCM-41 and SBA-1, Chem. Mater. 14 (2002) 4603–4610.
[14] J. Aguado, J.M. Arsuaga, A. Arencibia, Influence of synthesis conditions on mercury adsorption capacity of propylthiol functionalized SBA-15 obtained by co-condensation, Micropor. Mesopor. Mater. 109 (2008) 513–524.
[15] J. Dong, Z.H. Xu, F. Wang, Engineering and characterization of mesoporous silica-coated magnetic particles for mercury removal from industrial effluents, Appl. Surf. Sci. 254 (2008) 3522–3530.
[16] L.M. Guo, J.T. Li, L.X. Zhang, J.B. Li, Y.S. Li, C.C. Yu, J.L. Shi, M.L. Ruan, J.W. Feng, A facile route to synthesize magnetic particles within hollow mesoporous spheres and their performance as separable Hg^{2+} adsorbents, J. Mater. Chem. 18 (2008) 2733–2738.
[17] H. Tian, J.J. Li, Q. Shen, H.L. Wang, Z.P. Hao, L.D. Zou, Q. Hu, Using shell-tunable mesoporous Fe_3O_4@HMS and magnetic separation to remove DDT from aqueous media, J. Hazard. Mater. 171 (2009) 459–464.
[18] Y. Deng, D. Qi, C. Deng, X. Zhang, D. Zhao, Superparamagnetic high-magnetization microspheres with an Fe_3O_4@SiO_2 core and perpendicularly aligned mesoporous SiO_2 shell for removal of microcystins, J. Am. Chem. Soc. 130 (2008) 28–29.
[19] X. Chen, K.F. Lam, Q. Zhang, B. Pan, M. Arruebo, K.L. Yeung, Synthesis of highly selective magnetic mesoporous adsorbent, J. Phys. Chem. C 113 (2009) 9804–9813.
[20] J.F. Liu, Z.S. Zhao, G.B. Jiang, Coating Fe_3O_4 magnetic nanoparticles with humic acid for high efficient removal of heavy metals in water, Environ. Sci. Technol. 42 (2008) 6949–6954.
[21] R. Bai, C. Tien, Particle deposition under unfavorable surface interactions, J. Colloid Interface Sci. 218 (1999) 488–499.
[22] D. Zhao, J. Feng, Q. Huo, N. Melosh, G.H. Fredrickson, B.F. Chmelka, G.D. Stucky, Triblock copolymer syntheses of mesoporous silica with periodic 50 to 300 angstrom pores, Science 279 (1998) 548–552.
[23] J.M. Rosenholm, T. Czuryszkiewicz, F. Kleitz, J.B. Rosenholm, M. Lindén, On the nature of the Brønsted acidic groups on native and functionalized mesoporous siliceous SBA-15 as studied by benzylamine adsorption from solution, Langmuir 23 (2007) 4315–4323.
[24] J.M. Rosenholm, M. Lindén, Wet-chemical analysis of surface concentration of accessible groups on different amino-functionalized mesoporous SBA-15 silicas, Chem. Mater. 19 (2007) 5023–5034.
[25] L.L. Ji, W. Chen, L. Duan, D.Q. Zhu, Mechanisms for strong adsorption of tetracycline to carbon nanotubes: a comparative study using activated carbon and graphite as adsorbents, Environ. Sci. Technol. 43 (2009) 2322–2327.
[26] S. Deng, R. Bai, Adsorption and desorption of humic acid on aminated polyacrylonitrile fibers, J. Colloid Interface Sci. 280 (2004) 36–43.
[27] H. Salmio, D. Bruhwiler, Distribution of amino groups on a mesoporous silica surface after submonolayer deposition of aminopropylsilanes from an anhydrous liquid phase, J. Phys. Chem. C 111 (2007) 923–929.
[28] A.S. Maria Chong, X.S. Zhao, Functionalization of SBA-15 with APTES and characterization of functionalized materials, J. Phys. Chem. B 107 (2003) 12650–12657.
[29] Q. Tao, Z. Xu, J. Wang, F. Liu, H. Wan, S. Zheng, Adsorption of humic acid to aminopropyl functionalized SBA-15, Micropor. Mesopor. Mater. 131 (2010) 177–185.
[30] J. Magalhães, L. Moreira, U. Rodrigues-Filho, M. Giz, M. Pereira-da-Silva, R. Landers, R. Vinhas, P. Nascente, Surface chemistry of the iron tetraazamacrocycle on the aminopropyl-modified surface of oxidized *n*-Si (1 0 0) by AFM and XPS, Surf. Interface Anal. 33 (2002) 293–298.